LAWRENCE
LIVERMORE
NATIONAL
LABORATORY

UCRL-PROC-237301

Variable High Order Multiblock Overlapping Grid Methods for Mixed Steady and Unsteady Multiscale Viscous Flows

B. Sjogreen, H. C. Yee

December 17, 2007

International Conference on Spectral and High Order Methods
Beijing, China
June 18, 2007 through June 22, 2007

Disclaimer

Variable High Order Multiblock Overlapping Grid Methods for Mixed Steady and Unsteady Multiscale Viscous Flows

Björn Sjögreen* H. C. Yee†

November 7, 2007
Revised December 12, 2007

Abstract

Flows containing steady or nearly steady strong shocks in parts of the flow field, and unsteady turbulence with shocklets on other parts of the flow field are difficult to capture accurately and efficiently employing the same numerical scheme even under the multiblock grid or adaptive grid refinement framework. On one hand, sixth-order or higher shock-capturing methods are appropriate for unsteady turbulence with shocklets. On the other hand, lower order shock-capturing methods are more effective for strong steady shocks in terms of convergence. In order to minimize the shortcomings of low order and high order shock-capturing schemes for the subject flows, a multiblock overlapping grid with different orders of accuracy on different blocks is proposed. Test cases to illustrate the performance of the new solver are included.

*Center for Applied Scientific Computing, Lawrence Livermore National Laboratory,Livermore, CA 94551. sjogreen2@llnl.gov . This work performed under the auspices of the U.S. Department of Energy by Lawrence Livermore National Laboratory under Contract DE-AC52-07NA27344.

†NASA Ames Research Center, Moffett Field, CA94035 helen.m.yee@nasa.gov

1 Motivation

For nearly two decades, second and third-order shock-capturing schemes employing time-marching to the steady state have enjoyed much success in simulating many transonic, supersonic and hypersonic steady aeronautical flows containing strong shocks. In the presence of mixed steady and unsteady multiscale viscous flows, low order time-accurate methods are not effective in accurately simulating, e.g., unsteady turbulent fluctuation containing shocklets. At the same time, high order schemes with good unsteady shock-capturing capability suffer from the inability to converge to the proper steady shocks effectively. Attempts to improve the convergence rate of high order methods to strong steady shocks involve order reduction or added numerical dissipation of the scheme in the vicinity of the shocks, thus degrading the true order of the scheme in other parts of the flow.

Although extreme grid refinement can be accomplished on the unsteady turbulence part of the flow field, increases in instability and stiffness of the overall computations are inevitable. A method to effectively overcome these difficulties for mixed steady and unsteady viscous flows is a multiblock overlapping grid with a different order of numerical scheme on different block. Stable SBP (summation-by-parts) energy norm numerical boundary procedures for high order central schemes are employed at physical boundaries as well as at multiblock overlapping boundaries. Lagrangian interpolations are used to interpolate grid point values among the block overlapping regions. The logic in coding the resulting 3-D code is more complex as it deals with flexible grid stencil on multiblock interfaces. The following presents a description of the approach with some test cases to validate the solver without all the relevant physics included in the model. The next step is to apply the solver to practical applications. An important application for the proposed solver is to simulate blunt body space vehicles in hypersonic speed with strong steady or nearly steady bow shocks and possible complex turbulence/shocklet interaction near the wake region. Another application is in numerical modeling of the Heliosphere.

2 Overlapping grid hierarchies

Overlapping grids have a long history in computational fluid dynamics (CFD). For basic descriptions see [1].

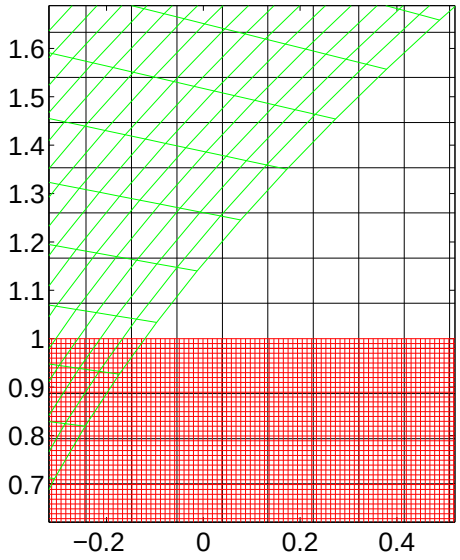

Figure 1: Three grids overlapping grids. The fine grid(red) and curvilinear grid(green) would be given higher priority than the coarse grid(black).

Fig. 2 shows a detail of an overlapping grid system where three component grids meet. In regions of overlap, one grid, the grid with highest priority, carries the computed solution and parts of other grids in the same region are cut away. In Fig. 2 the coarsest grid(black) would normally be given the lowest priority, and the parts of it that are covered by the fine grid (red) or the curvilinear grid (green) would be unused. The boundaries of the uncovered regions of the grids obtain values by interpolation from other grids. The interpolation is always two way. At the interface between two grids, say G_1 and G_2, the boundary of G_1 interpolates from G_2 and the boundary of G_2 interpolates from G_1. The interpolation can be implicit or explicit. In explicit interpolation, the points in G_2 that are used in the interpolation stencil for computing values at the boundary of G_1 are not allowed to be interpolation points. In implicit interpolation, interpolation points on one grid are allowed to be part of the interpolation stencil from the other grid. Implicit interpolation allows a smaller size overlap between the grids, but it is necessary to solve an algebraic system of equations for the interpolation values. Fig. 2 depicts explicit and implicit interpolation for a one dimensional example.

For a discretization with finite difference operators of stencil width $2s+1$,

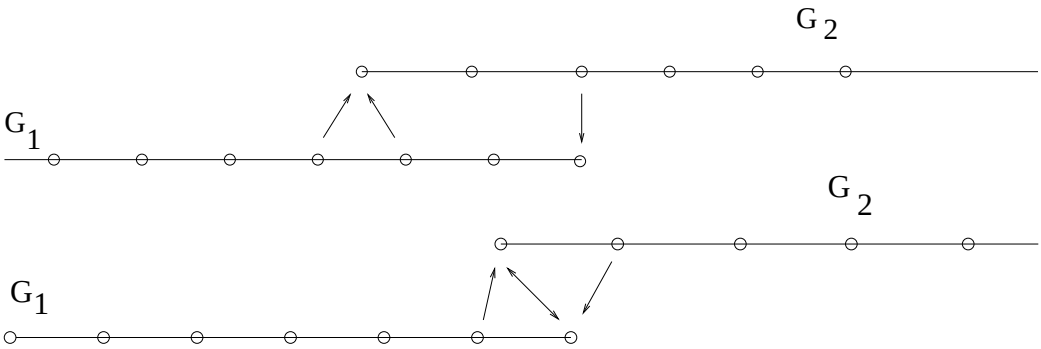

Figure 2: Interpolation between grids in one space dimension. Explicit (top) and implicit (bottom) interpolation.

we use s layers of interpolation points at the interpolation boundaries of the grids. No other boundary conditions except for interpolation are needed. It would have been possible to use summation by parts boundary operators to decrease the number of layers of interpolation points, but here we only use summation by parts operators at the real physical boundaries.

Overlapping grid generators such as Xcog [4] or Ogen [3], cut away underlying grids and determine which points needs to be interpolated from other component grids. They output interpolation information in the form of a table. The user inputs the stencil width of the difference scheme he wants to use and the stencil with of the interpolation stencil he wants to use. For example, three layers of interpolation points are needed with a sixth order difference operator.

We use Lagrangian interpolation between component grids. If the point (i, j, k) in grid g is interpolated from grid g_f with a stencil whose lower left corner is (i_f, j_f, k_f), and the location of (i, j, k) in the parameter space of g_f is (c_i, c_j, c_k), then the $r + 1$th order interpolation formula is

$$u^{(g)}_{i,j,k} = \sum_{l=0}^{r} \sum_{m=0}^{r} \sum_{n=0}^{r} L_l(c_i) L_m(c_j) L_n(c_k) u^{(g_f)}_{i_f+l, j_f+m, k_f+n} \tag{1}$$

where $u^{(g)}_{i,j,k}$ is the solution on grid g at grid point (i, j, k). The standard

Lagrange polynomial basis is

$$L_l(\xi) = \prod_{\substack{p=0 \\ p \neq l}}^{r} \frac{\xi - x_{i_f+p}}{x_{i_f+l} - x_{i_f+p}},$$

and similarly for the j and k directions.

The overlapping grid system enables us to use different numerical schemes on different component grids. The stencil width input to the grid generator is the maximum width over all discretizations that potentially will be used for any component grid. Higher order schemes require higher order interpolation between component grids. The interpolation stencil width, i.e., r be in (1), in the overlapping grid system must be chosen to permit interpolation of high enough order.

3 Data structure and message passing

For parallel execution using message passing, we distribute each component grid evenly on the total number of processors available. This gives perfect load balancing, but the amount of communication is larger than optimal. However, because we use explicit time stepping, the communication cost is still only a small fraction of the total computation time. The approach is most efficient when the composite grid is made up of a few large component grids, because of low computation to communication ratio when component grids with very few grid points are distributed on a large number of processors.

Information about interpolation arrives from the grid generation program in a table with entry $(\mathbf{i}, g, \mathbf{i}_f, g_f, \mathbf{c}_f)$ for each interpolation point. The meaning is that the point with index $\mathbf{i}$ in grid g, should interpolate from grid g_f, with an interpolation stencil that has point $\mathbf{i}_f$ as lower left corner and $\mathbf{c}_f$ is the location of point $\mathbf{i}$ in the curvilinear coordinate system g_f.

The whole interpolation table is read into each processor and split into one "get from" table representing interpolation points owned by the processor and one "give to" table representing values that needs to be interpolated in the processor. The entries in the "get from" table are $(\mathbf{i}, g, p)$ meaning that point $\mathbf{i}$ in grid g is an interpolation point that should get its value from processor p. The entries in the "give to" table are $(\mathbf{i}_f, g_f, \mathbf{c}_f, p)$, meaning that a value located at parameter values $\mathbf{c}_f$ in grid g_f should be interpolated with point $\mathbf{i}_f$ as lower left corner and then sent to processor p.

The "get from" and "give to" tables are built in the same order as the original non-parallel table. Therefore, if the interpolated values are sent in the order of the "give to" table from processor p they will be received in the right order in processor q. For example, if the first entry in processor ps "give to" table says that the interpolated value should be sent to processor q, then the first entry with processor p in the "get from" table in processor q is the corresponding point.

The tables are represented in such a way that all communication that is associated with the interpolation is done with a single call to the MPI function `MPI_Alltoallv`.

4 Equations and numerical method

We solve the compressible Navier-Stokes equations in non-dimensional units,

$$\begin{aligned} \rho_t + \operatorname{div} \rho\mathbf{u} &= 0 \\ (\rho\mathbf{u})_t + \operatorname{div}(\rho\mathbf{u}\mathbf{u}^T + pI) &= \operatorname{div}\tau \\ e_t + \operatorname{div}\mathbf{u}(e+p) &= \operatorname{div}(\tau : D) + \operatorname{div}\mathbf{q} \end{aligned} \tag{2}$$

The dependent variables are the density, ρ, the velocity (column) vector, $\mathbf{u}$, and the total energy e. Superscript T denotes matrix transpose, and I is the 3×3 identity matrix. p denotes the pressure and the 3×3 matrix D is the symmetric part of the velocity gradient,

$$D_{ij} = \frac{1}{2}\left(\frac{\partial u_i}{\partial x_j} + \frac{\partial u_j}{\partial x_i}\right)$$

The viscous tensor is is given by

$$\tau = \frac{\alpha(T)}{Re}(-\frac{2}{3}\operatorname{div}\mathbf{u}I + 2D)$$

and the heat conduction is given by

$$\mathbf{q} = \frac{\alpha(T)\gamma}{RePr(\gamma-1)}\nabla\frac{p}{\rho}.$$

The tensor product of two matrices is defined as

$$A : B = \sum_{i=1}^{3}\sum_{j=1}^{3} a_{i,j}b_{i,j}.$$

Re denotes the Reynolds number, Pr is the Prandtl number, γ is the c_p to c_v ratio, and $\alpha(T)$ is the viscosity temperature dependency. The temperature is computed as

$$T = \frac{Mp}{R\rho}.$$

The constants M and R are the molar mass of the gas and the universal gas constant respectively. In the computations below, we will give a free stream state (denoted by subscript ∞) and determine M/R by $M/R = T_\infty \rho_\infty / p_\infty$. For viscous computations, we will use Sutherland's law,

$$\alpha(T) = \left(\frac{T}{T_\infty}\right)^{1.5} \frac{T_\infty + 110}{T + 110}.$$

For inviscid computations, we will use

$$\alpha(T) = 0.$$

On some component grids we discretize (2) by a sixth order accurate finite difference scheme with summation-by-parts boundary modification of the difference operators. This is discretization is the same as the base scheme described in [6]. On other component grids we discretize the convective terms in (2) by second order accurate TVD type scheme with the minmod limiter. We use a fourth order Runge-Kutta method to advance the solution in time. When the solution is in a steady (or quasi-steady) state, we time march first with the TVD scheme on all grids, and later when the solution is fully developed, switch to sixth order accurate scheme on some of the component grids. When the discretizations are mixed with TVD approximations on some grids and centered sixth order approximations on some grids, we use the fourth order Runge-Kutta method on all grids.

5 Numerical tests

We present a few simple tests to demonstrate that the method works, and we show the improvement in accuracy when switching to a high order centered scheme on component grids that do not have any strong shocks.

We used the overlapping grid generator Xcog [4] to generate the two dimensional overlapping grids. For three space dimensions, we used the Ogen

grid generator [3]. The grids were generated with an overlap that allows evaluation of nine point stencils, required for the eight order artificial dissipation term in our sixth order accurate centered scheme. Unless otherwise stated, the width of the interpolation stencil is five points, which means the interpolation is fifth order accurate. The interpolation is explicit in all computations below.

5.1 Accuracy of inviscid flow, error propagation from a bow shock

We consider inviscid flow with free stream Mach number 3 past a cylinder with radius 0.5. γ is 1.4. It is well known that the presence of a shock can reduce the actual convergence rate when the grid spacing goes to zero to first order even when using numerical method of formally high order of accuracy [2]. We here study this effect in the context of high order methods with SBP boundary conditions as described in [6].

The flow in the wake region depends strongly on the viscosity. Therefore, we do not consider the wake for this inviscid computation, and we use the two overlapping grids shown in Fig. 3. On the grid at the shock, we use a TVD difference scheme, on the grid around the cylinder, we will use a 6th order accurate scheme. For comparison we will also compute with a TVD difference scheme on both grids. We will compare three different grid refinements, the coarsest overlapping grid has 81×43 (cylinder) and 155×55 (shock) points. The next finer grid has 161×85 and 301×109 points, and the finest grid has 321×169 and 601×217 points. Results on these three overlapping grids are labeled by h, $h/2$, and $h/4$ in Figs. 4 and 5 below.

For inviscid flows, the entropy is constant on the streamlines, with possible jumps at the shocks. With knowledge of the free stream state, we can compute analytically, by the Rankine-Hugoniot conditions, the entropy on the streamline that coincides with $y = 0$ in the free stream. This streamline passes normally through the bow shock, and attaches to the body of the cylinder. We will use the error in entropy along the body as a measure of accuracy.

In Fig. 4 we display the entropy error along the streamline for inviscid flow with 2nd order TVD scheme at the shock grid and 6th order accurate centered scheme. Fig. 4 shows that the error decreases with a first order accurate convergence rate. This is most likely due to errors that propagate

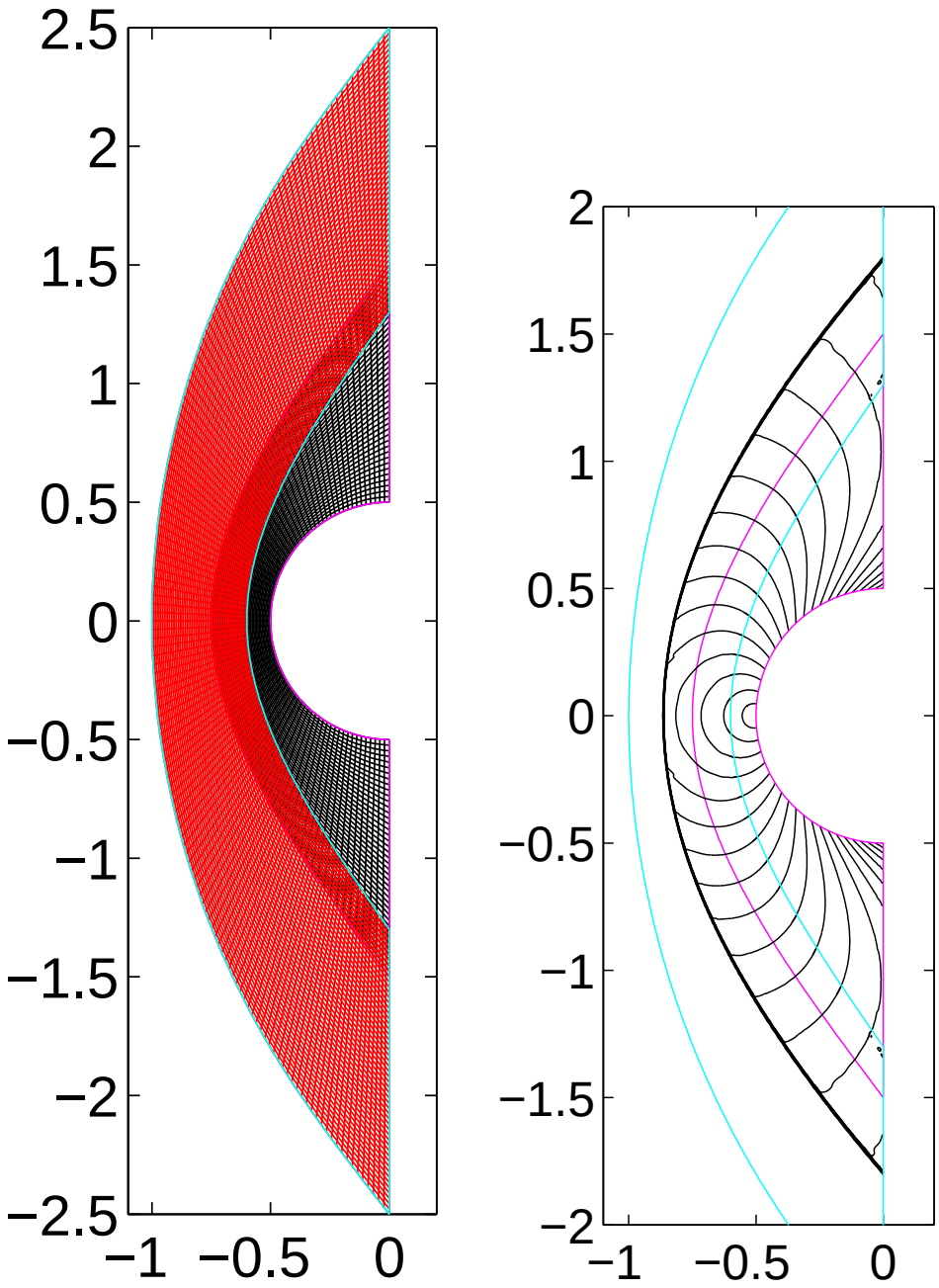

Figure 3: Two overlapping grids for inviscid computation (left). Computed flow field at stream Mach number three (right).

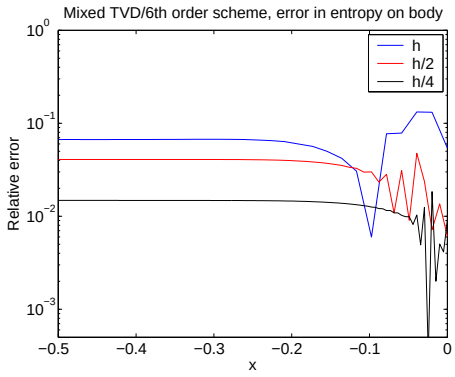

Figure 4: Relative error in entropy on cylinder as function of x. Mixed TVD and 6th order. (81×43,155×55) grid points (blue), (161×85,301×109) grid points (red), and (321×169,601×217) grid points (black).

from the bow shock, [2]. The behavior of the error with time is that a quasi steady state is reached around the dimensionless time 10, where the error is considerably smaller than the steady state errors shown in Fig. 4. The error then increases to the level shown in Fig. 4 where a steady state seems to have been reached. Nevertheless, the error in absolute terms is much smaller than the error from using only the TVD difference scheme, shown in Fig. 5. The computations in Fig. 5 were made with third order accurate interpolation between the component grids. Furthermore, when solving the Navier-Stokes equations we expect the physical viscosity to smooth the discontinuities to make the effect of error propagation from shocks smaller.

We conclude that mixing a high order method with a TVD scheme gives a significantly smaller error than obtained with only the TVD difference scheme, but that the high order convergence rate is not obtained.

5.2 Accuracy of viscous flow, the skin friction coefficient

We consider viscous flow with free stream Mach number 3 and Reynolds number 500 past a cylinder with radius 0.5. The Prandtl number is 0.72, γ is 1.4, $T_\infty = 273.15K$.

The domain is discretized by the overlapping grid configuration displayed in Fig. 6. There are four grids, a base grid that covers the entire domain, a

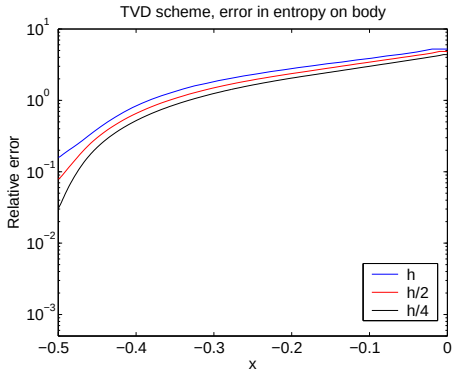

Figure 5: Relative error in entropy on cylinder as function of x. TVD scheme on both component grids. (81×43,155×55) grid points (blue), (161×85,301×109) grid points (red), and (321×169,601×217) grid points (black).

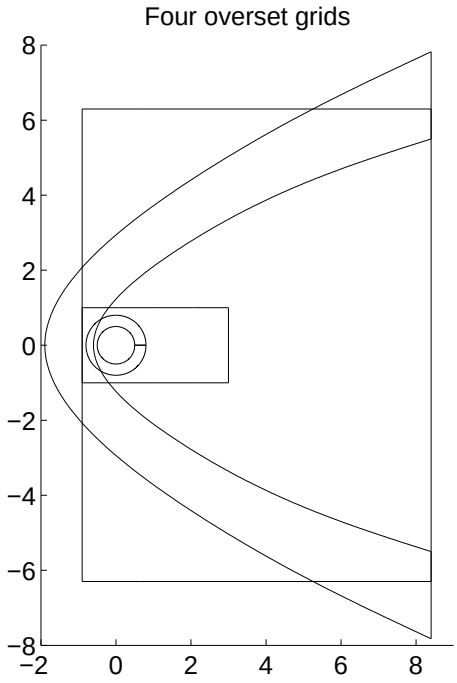

Figure 6: Overlapping grid domains used for computations with body fitted grids.

	Coarse	Medium	Fine
base grid	100x136	200x272	200x272
wake grid	400x200	800x400	1200x600
shock grid	160x35	320x70	320x70
body grid	352x15	697x30	1387x60

Table 1: Number of grid points in composite grids for the three computations. The body grid and the wake grid have cell aspect ratios close to one.

curved grid around the bow shock, a fine polar grid near the cylinder surface, and a fine grid that covers the wake region.

We compare solution on three different composite grids, Coarse, Medium, and Fine. Table 1 gives the number of grid points in these grids. The thickness of the cylinder grid in the radial direction is 0.1, the number of grid points are chosen such that the grid spacing is of the similar size radially and tangentially. The size of the wake grid is such that the grid spacing is of similar size as the spacing of the cylinder grid. The finest grid has discretization step $h = 1.7 \times 10^{-3}$ in the radial direction, which gives 26 grid points over the width $1/\sqrt{Re}$ for Reynolds number 500.

Fig. 7 shows local Mach number contours of a solution computed on the Medium grid. The grid boundaries are outlined in color (or gray). The close up to the right shows good agreement of the contour lines between the component grids. The structure in the wake, and the trailing discontinuities can be completely resolved by the centered scheme and the physical viscosity, no artificial dissipation is needed. This is not the case for the bow shock, which is unresolved even on the finest grid. To assess the accuracy of the computations, we plot the skin friction coefficient along the body,

$$C_f = \frac{\alpha(T)}{Re} \frac{1}{\frac{1}{2}\rho_\infty U_\infty^2} \frac{\partial V}{\partial n}, \tag{3}$$

where V denotes the tangential velocity on the boundary.

Fig. 8 shows the skin friction coefficient on the three different grids when a sixth order accurate method is used on all grids except on the grid around the bow shock. Fig. 9 shows C_f for the same computations, but with the TVD difference scheme on all grids. It is clearly seen that the mixed sixth order/TVD method converges faster than the pure TVD method. Both methods converge to the same C_f curve.

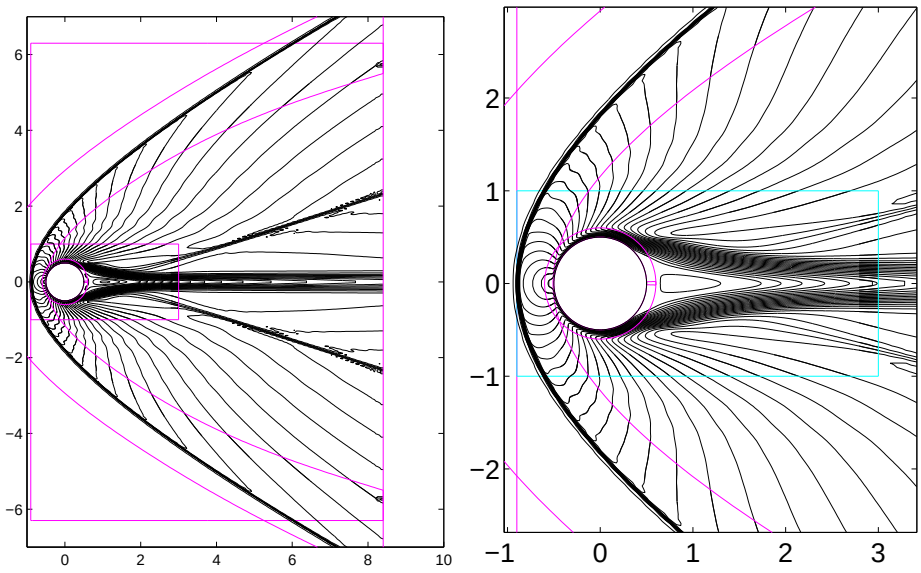

Figure 7: Solution on overlapping grids for Mach=3 and Re=500. Mach number contours. 6th order accurate scheme on all grids except the bow shock grid. Right plot is a close up of the region near the cylinder.

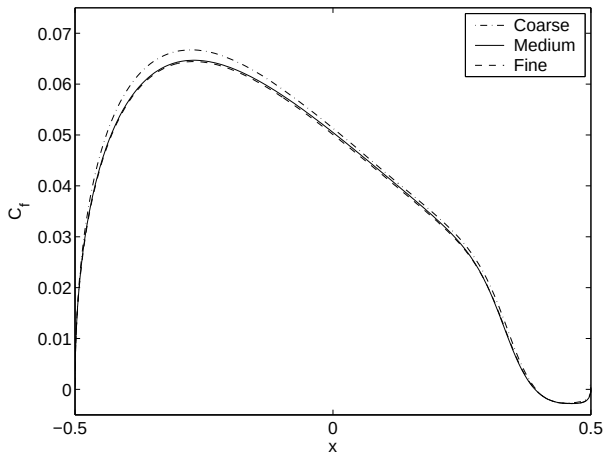

Figure 8: C_f as function of x along the cylinder surface. Three overlapping grids of increasing refinements.

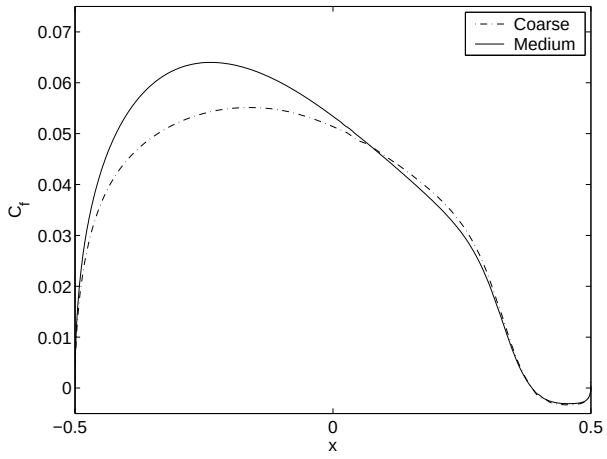

Figure 9: C_f as function of x along the cylinder surface. Three overlapping grids of increasing refinements.

5.3 Three dimensional example

We study the flow past a re-entry vehicle. The geometry with overlapping grid system is outlined in Fig. 10. There are six grids in total. The Cartesian background grid, in blue color in Fig. 10, has a fairly coarse grid spacing, The body is defined by a spline curve, rotated around the x-axis (magenta) with two orthographic cap grids (light blue and dark blue) that cover the polar singularities. A cylindrical grid (green) together with a Cartesian grid (red) that covers its polar singularity are inserted in the wake region. The grid spacing is approximately 0.05 on the body and wake grids, about five times larger on the Cartesian background grid. The flow conditions are the same as used for the Fire II configuration in [5]. The free stream Mach number is 16 and the free stream temperature is 237 K.

A computed inviscid flow field is shown in Fig. 11.

6 Conclusions

We have described an extension of our previously developed high order schemes to geometries discretized by overlapping grids. We have shown example computations where high order schemes are used on some of the component grids, and shock capturing schemes are used on other component

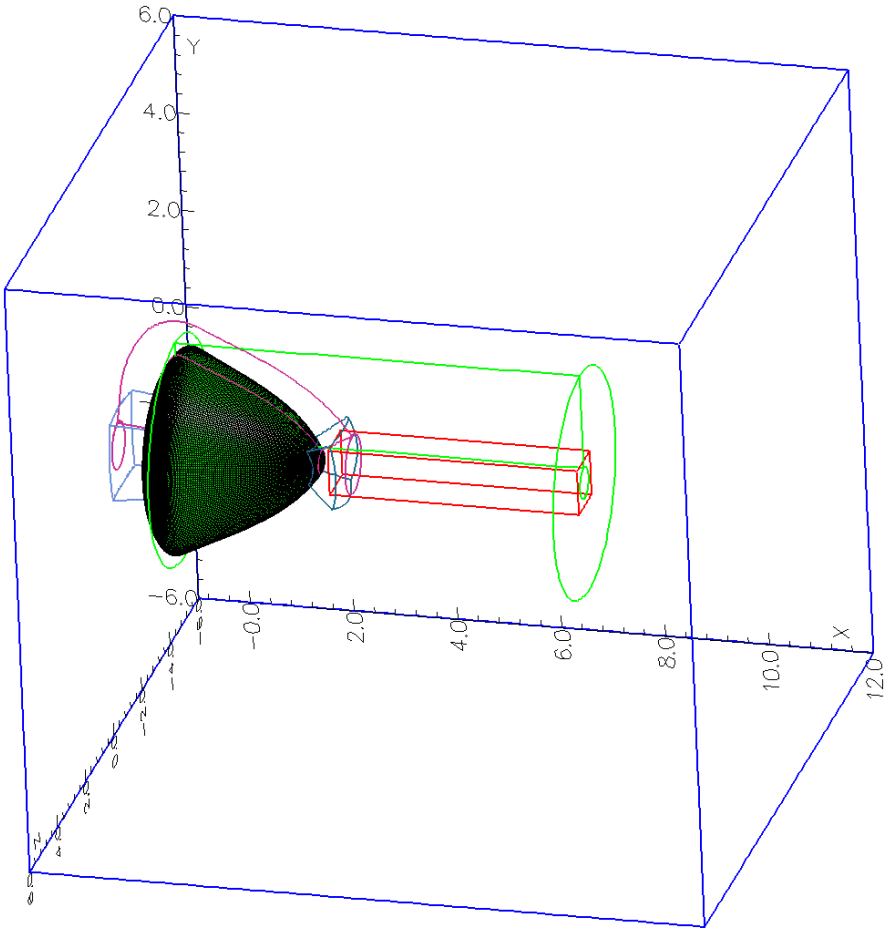

Figure 10: Overlapping grid system for re-entry vehicle computation.

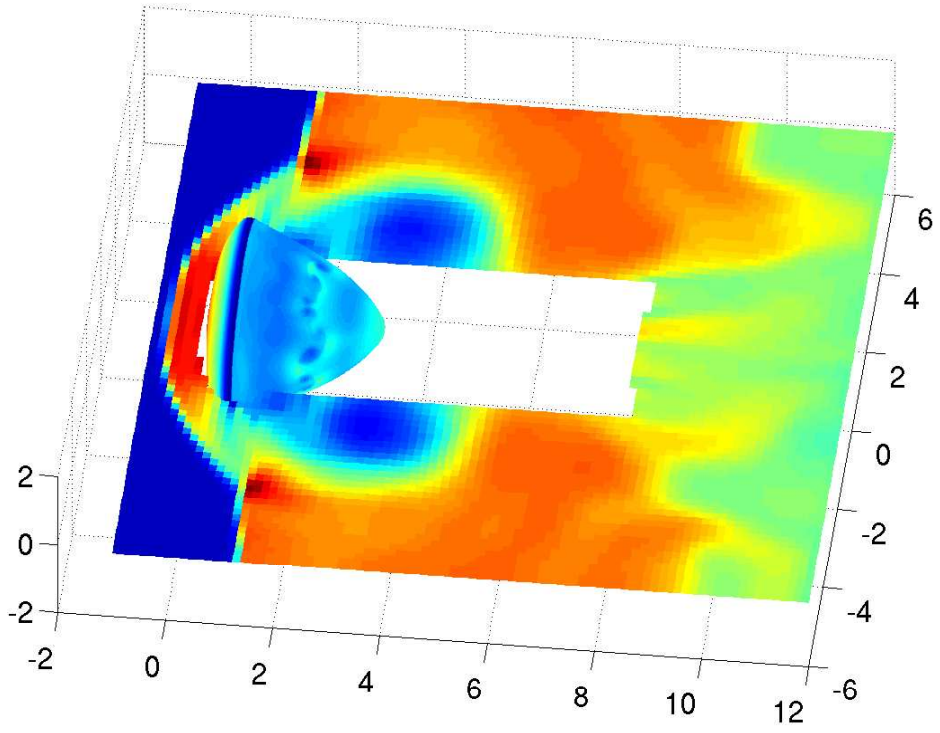

Figure 11: Density color levels, inviscid computation.

grids. We have given examples that show that the error in high speed flow computations, is significantly smaller when high order schemes are used on some component grids.

Many questions regarding error propagation for shock problems remains to be answered. Future plans include a more extensive study of such phenomena in practical settings. For example it would be possible to use a higher order shock capturing scheme (e.g., a WENO method) around the bow shock.

The three dimensional re-entry computations will be extended with the objective to study the flow, and how the flow is affected by the order of accuracy of the scheme, in the wake region for moderate and high Reynolds numbers.

7 Acknowledgments

We thank Bill Henshaw at Lawrence Livermore National Laboratory for help with the Ogen grid generator.

References

[1] G. Chesshire and W.D. Henshaw. Composite overlapping meshes for the solution of partial differential equations. *J. Comput. Phys.*, 90(1):1–64, 1990.

[2] B. Engquist and B. Sjögreen. The convergence rate of finite difference schemes in the presence of shocks. *SIAM J. Numer. Anal.*, 35:2464–2485, 1998.

[3] W.D. Henshaw. Ogen: An overlapping grid generator for Overture. Research Report UCRL-MA-132237, Lawrence Livermore National Laboratory, 1998.

[4] N. Anders Petersson. An algorithm for assembling overlapping grid systems. *SIAM J. Sci. Comput.*, 20(6):1995–2022, 1999.

[5] Krishnendu Sinha, Michael Barnhardt, and Graham V. Candler. Detatched eddy simulation of hypersonic base flows with application to Fire

II experiments. Paper 2004-2633, AIAA, June 2004. 34th AIAA Fluid Dynamics Conference and Exhibit, Portland, Oregon.

[6] B. Sjögreen and H. C. Yee. Multiresolution wavelet based adaptive numerical dissipation control for shock-turbulence computation. *J. Sci. Comp.*, 20:211–255, 2004.